

Correlation dimension and phase space contraction via extreme value theory

Davide Faranda^{1,a)} and Sandro Vaienti^{2,b)}

¹LSCE-IPSL, CEA Saclay l'Orme des Merisiers, CNRS UMR 8212 CEA-CNRS-UVSQ,
 Université Paris-Saclay, 91191 Gif-sur-Yvette, France

²Aix Marseille Univ., Université de Toulon, CNRS, CPT, 13009 Marseille, France

(Received 1 March 2018; accepted 10 April 2018; published online 30 April 2018)

We show how to obtain theoretical and numerical estimates of correlation dimension and phase space contraction by using the extreme value theory. The maxima of suitable observables sampled along the trajectory of a chaotic dynamical system converge asymptotically to classical extreme value laws where: (i) the inverse of the scale parameter gives the correlation dimension and (ii) the extremal index is associated with the rate of phase space contraction for backward iteration, which in dimension 1 and 2, is closely related to the positive Lyapunov exponent and in higher dimensions is related to the metric entropy. We call it the Dynamical Extremal Index. Numerical estimates are straightforward to obtain as they imply just a simple fit to a univariate distribution. Numerical tests range from low dimensional maps, to generalized Henon maps and climate data. The estimates of the indicators are particularly robust even with relatively short time series. Published by AIP Publishing. <https://doi.org/10.1063/1.5027386>

This study uses the link between extreme value laws and dynamical systems theory to show that important dynamical quantities as the correlation dimension, the entropy, and the Lyapunov exponents can be obtained by fitting observables computed along a trajectory of chaotic systems. All this information is contained in a newly defined Dynamical Extremal Index. Besides being mathematically well defined, it is almost numerically effortless to get as (i) it does not require the specification of any additional parameter (e.g., embedding dimension, decorrelation time); (ii) it does not suffer from the so-called curse of dimensionality. A numerical code for its computation is provided in the supplementary material.

I. INTRODUCTION

Since its introduction by Grassberger and Procaccia,^{1,2} the correlation dimension (CD) has been used as a powerful indicator for the description of the fractal structure of invariant sets in dynamical systems. Similarly, the Lyapunov exponents and the entropy^{3,4} provide an indication of the relevant time scales associated with the dynamics and the predictability horizon of the system. Given the importance of these quantities, there exists an increasing body of literature on how to estimate CD, Lyapunov exponents, and entropy. It has been shown that reliable estimates of CD can be obtained with relatively short time series.⁵ Instead, the computations of Lyapunov exponents and entropy are still challenging because the existing methodologies require as input additional parameters as the embedding dimension and the relevant time scale of the dynamics (e.g., the decorrelation time). Calculations are limited to the top Lyapunov exponent

and the reliability of estimates from the time series of experimental phenomena is often questioned.⁶ We defer the reader to the monographs^{7,8} and to the articles^{9,10} for recent advancements on the various statistical tools to investigate the nonlinear time series.

The extreme value theory (EVT) has been used to characterize the evolution of chaotic systems.^{11,12} It is possible to obtain dynamical properties in phase space (fractal dimension or stability) by exploiting the limiting theorems of the extreme value theory. The main idea is: (i) to replace the stochastic processes used in the statistical framework with a trajectory of a chaotic dynamical system and (ii) to study the convergence of maxima of suitable observables to the classical extreme value laws. The parameters of the EVT provide estimates of dynamical properties of the system. This connection between EVT and the dynamical properties of chaotic systems is rich not only from a theoretical but also from a numerical perspective. Indeed, the estimates of local properties obtained with EVT do not require the introduction of additional parameters and they are easy to implement numerically. They have been used to get insights into the dynamical behavior of atmospheric flows in Refs. 13–15. In Ref. 16, it has been shown that the numerical algorithm based on EVT provide reliable estimates of the dimension of high dimensional systems up to phase spaces with thousands of dimensions. It is therefore desirable to estimate other key dynamical quantities in the EVT framework.

The purpose of this communication is to show that the correlation dimension and the EVT are intimately related: the CD arises by studying the distribution of the maxima of a new suitable observable evaluated along the orbit of a chaotic system. Moreover, an exponent of the limit law, the extremal index, is related, for hyperbolic attractors, to the positive Lyapunov exponent in dimension two and to the metric entropy in higher dimensions. The idea of the relationship between EVT and CD comes from a previous

^{a)}Also at London Mathematical Laboratory, 14 Buckingham Street, London WC2N 6DF, United Kingdom. Electronic mail: davide.faranda@cea.fr

^{b)}Electronic mail: vaienti@cpt.univ-mrs.fr

work¹⁷ where we used the extreme value theory to detect and quantify the onset of synchronization in coupled map lattices. The relationship between the extremal index and the Lyapunov exponent and the entropy is new and is particularly striking for maps with piecewise constant jacobian. In the general case, we derive a formula whose validity is confirmed by numerical experiments. We also explain the relation between our extremal index, the local dimensions, and the phase space contraction. In the rest of the paper, we will name it as the DEI, the *dynamical extremal index*. We want to point out that our DEI is a well defined quantity that can be used as a new indicator for the sensitivity associated with local hyperbolicity. We will present the theoretical results in Sec. II: some of those results can be obtained by generalizing the techniques introduced in Ref. 17; we will also address the need to develop a more appropriate theory of EVT for diffeomorphisms in higher dimensions. We will then provide several examples of classical conceptual low-dimensional dynamical systems. We will discuss the implications of our results on higher dimensional systems and the possibility to apply them to more general time series. As an example, we will compute the indicators on climate data and explain how they provide relevant physical information on the atmospheric circulation over the North Atlantic.

II. THEORETICAL RESULTS

A. A brief presentation of the extreme value theory and a new observable

Let (M, μ, T) be dynamical systems given by a map T acting on the metric compact space M with distance $d(\cdot, \cdot)$ and preserving the Borel measure μ . Usually, M will be a compact subset of some \mathbb{R}^n and d a distance equivalent to the standard one. Let us take the *direct product* $(M \times M, \mu \times \mu, T \times T)$, and denote with $(x, y) \in M \times M$, a couple of point in the Cartesian product $(M \times M)$. We then introduce the observable $\psi(x, y) = -\log d(x, y)$, and consider the process $\{\psi \circ (T^j \times T^j)\}_{j \geq 0}$, and the maximum of the sequence $\mathcal{M}_n(x, y) = \max\{\psi(x, y), \psi(Tx, Ty), \dots, \psi(T^{n-1}x, T^{n-1}y)\}$ and finally its distribution $\mathbb{P}(\mathcal{M}_n \leq u_n)$, where $\mathbb{P} = \mu \times \mu$ is the underlying probability and u_n is a suitable scaling function tending to infinity and which we are going to define. Suppose that for a given positive number τ we can find a sequence of numbers u_n such that $n\mathbb{P}(\psi \geq u_n) \rightarrow \tau, n \rightarrow \infty$. We say, that the process $\{\psi \circ (T^j \times T^j)\}_{j \geq 0}$ satisfies an extreme value law of Gumbel's type if there is a number $\theta \in (0, 1]$, the *extremal index*, such that $\mathbb{P}(\mathcal{M}_n \leq u_n) \rightarrow e^{-\theta\tau}, n \rightarrow \infty$. We now introduce the diagonal neighborhood S_n in the product space: $S_n = \{(x, y), d(x, y) \leq e^{-u_n}\}$. By substituting the expression of ψ in $\mathbb{P}(\psi \geq u_n)$, we have

$$\mathbb{P}(\psi \geq u_n) = \mathbb{P}((x, y) \in S_n) = \int_M \mu(B(x, e^{-u_n}))d\mu(x), \tag{2.1}$$

where $B(x, a)$ denotes the ball of radius a centered on x . (Actually, we got the equality of the right hand side in the limit of large n when the two small corners of S_n become negligible.) The quantity $\int_M \mu(B(x, r))d\mu(x)$ scales like r^{D_2}

and the exponent D_2 is called the *correlation dimension* and it characterizes the fractal structure of the support of μ ; a more formal, definition of this fact is given in Ref. 18, Sec. 17, and references therein. A precise definition consists in taking the limsup and liminf of the ratio of the logarithm with $\log(1/r)$. By injecting successively into (2.1), we have therefore that for large n

$$u_n \sim \frac{-\log \tau}{D_2} + \frac{\log n}{D_2} := \frac{z}{a_n} + b_n, \tag{2.2}$$

where $\tau = e^{-z}$, $a_n = D_2$ and $b_n = \frac{\log n}{D_2}$. For numerical purposes, distribution functions like $\mathbb{P}(\mathcal{M}_n \leq z)$ are modelled, for n sufficiently large, by the so-called *generalized extreme value (GEV)* distribution which is a function depending upon three parameters $\xi \in \mathbb{R}, \kappa \in \mathbb{R}, \sigma > 0$ and such that:

$$F_{\text{GEV}}(z; \kappa, \sigma, \xi) = \exp\left\{-\left[1 + \xi\left(\frac{z-\kappa}{\sigma}\right)\right]^{-1/\xi}\right\}.$$

The parameter ξ is called the tail index; when its value is 0, the GEV corresponds to the Gumbel type. The parameter κ is called the location parameter and σ is the scale parameter: for n large, the scaling constant a_n is close to σ^{-1} and b_n is close to κ . Therefore, if we could fit a limit law of Gumbel's type with suitable normalizing parameters a_n and b_n , we immediately get the correlation dimension. Such a technique was previously used with a different observable, and it allowed to get the so-called *information dimension* $D_1(x)$, another fractal dimension which provides the scaling of the measure of a ball around a given point x , see Ref. 19 and references therein. Although the information dimension depends on the point x , its value is the same for almost all the choices of x with respect to the invariant measure and such an averaged valued, simply D_1 , is larger or equal to D_2 , see Ref. 20 for an account on the different fractal dimensions. In particular, if we denote with d_H the Hausdorff dimension, we have $D_2 \leq D_1 \leq d_H$.

B. The spectral approach with the new observable for conformal repellers

Before showing our numerical simulations for the computation of the CD, let us argue how we get a Gumbel type asymptotic distribution with an extremal index θ of dynamical meaning. First, we consider one-dimensional dynamical systems generated by uniformly expanding maps with an invariant set which could be a Cantor set and equipped with mixing Gibbs measures. These systems are better known as *conformal repellers*,—see for instance²¹ for a recent contribution—whose measures are characterized by a potential φ of type $\varphi(x) = -\beta \log |T'(x)|$, where T' denotes the derivative of T and $\beta \in \mathbb{R}$. If we denote them as μ_β , they are given by $h_\beta \nu_\beta$, where the density h_β and the *conformal* measure ν_β are, respectively, the eigenfunctions of the transfer operator (Perron-Fröbenius) and of its dual, both with eigenvalue $\lambda_\beta = e^{Q(\beta)}$, being $Q(\beta)$ the topological pressure. We remind that the transfer operator \mathcal{P}_T for the map T is defined, for an observable f in some suitable Banach space \mathcal{B} —for instance the space of Lipschitz continuous functions—by the duality relation: $\int \mathcal{P}_T f d\nu_\beta = \lambda_\beta \int f d\nu_\beta$. We defer to the monograph²²

for an introduction to thermodynamic formalism. The conformal measure verifies the property $\nu_\beta(TA) = \lambda_\beta \int_A e^{-\varphi} d\nu_\beta$, where T is one-to-one over the measurable set A . A powerful method to investigate the distribution of our process $\{\psi \circ (T^j \times T^j)\}_{j \geq 0}$ consists in perturbing the transfer operator \mathcal{P} of the direct product $T \times T$. The key observation is that by repeatedly using the duality relation, we can write $\mathbb{P}(\mathcal{M}_n \leq u_n) = \lambda_\beta^{-2n} \int \int \tilde{\mathcal{P}}_n^n(h_\beta(x)h_\beta(y))d\nu_\beta(x)d\nu_\beta(y)$, where the perturbed operator $\tilde{\mathcal{P}}_n$ is defined by acting on observables $f \in \mathcal{B}$, as $\tilde{\mathcal{P}}_n(f) = \mathcal{P}(f\mathbf{1}_{S_n^c})$, and $S_n = \{(x, y); d(x, y) \leq e^{-u_n}\}$. When n tends to infinity, the characteristic function of the complement of S_n , $\mathbf{1}_{S_n^c}$, goes to the identity and the operators \mathcal{P} and $\tilde{\mathcal{P}}_n$ converge to each other in \mathcal{B} . If the unperturbed operator \mathcal{P} has a spectral gap, it allows exponential mixing for the observables in \mathcal{B} . This compensates the lack of independence of the process $\{\psi \circ (T^j \times T^j)\}_{j \geq 0}$. The same is true for the operator $\tilde{\mathcal{P}}_n$ and the maximal, isolated, eigenvalue of \mathcal{P} , λ_β^2 , is close to that of $\tilde{\mathcal{P}}_n$, $\tilde{\lambda}_{\beta,n}^{(2)}$. More precisely: $\tilde{\lambda}_{\beta,n}^{(2)} \sim \lambda_\beta^2 - (1 - \lambda_\beta^2 q_0)\mathbb{P}(S_n)$, where now $\mathbb{P} = \mu_\beta \times \mu_\beta$. We will define the factor q_0 in a moment. The operator $\tilde{\mathcal{P}}_n$ now decomposes as the sum of a projection along the one dimensional eigenspace associated with the eigenvalue $\tilde{\lambda}_{\beta,n}^{(2)}$ and an operator with a spectral radius exponentially decreasing to zero and which can be neglected in the limit of large n . This allows us to write $\mathbb{P}(\mathcal{M}_n \leq u_n) \sim \lambda_\beta^{-2n} \tilde{\lambda}_{\beta,n}^{(2)n} \int \int h_\beta(x)h_\beta(y)d\nu_{\beta,n}(x)d\nu_{\beta,n}(y)$, where $\nu_{\beta,n}$ is the conformal measure for the perturbed operator and the double integral on the right hand side converges to 1 for $n \rightarrow \infty$. Finally, we get by approximating $\tilde{\lambda}_{\beta,n}^{(2)}$ as above: $\mathbb{P}(\mathcal{M}_n \leq u_n) \sim \left[1 - \frac{(1-\lambda_\beta^2 q_0)\mathbb{P}(S_n)}{\lambda_\beta^2}\right]^n \sim \exp\left[-\frac{(1-\lambda_\beta^2 q_0)\mathbb{P}(S_n)}{\lambda_\beta^2}n\right]$. We now remind that we are under the assumption that $n\mathbb{P}(\psi \geq u_n) = n\mathbb{P}(S_n) \rightarrow \tau, n \rightarrow \infty$. This lead to the Gumbel law $e^{-\theta\tau}$ provided that the dynamical extremal index θ is defined as

$$\theta = \frac{1 - \lambda_\beta^{-2} q_0}{\lambda_\beta^2}. \tag{2.3}$$

The term q_0 is obtained by the previous perturbation theory under the assumption that the diagonal in the product space is left invariant by the direct product of the two maps. In particular, we have

$$q_0 = \lim_{n \rightarrow \infty} \frac{\mathbb{P}(S_n \cap \tilde{T}^{-1}S_n)}{\mathbb{P}(S_n)}, \tag{2.4}$$

provided that the limit exists. The technique just described was first proposed by Keller²³ as an alternative way to get EVT for systems with exponential mixing and it is based on a perturbative result by Keller and Liverani.²⁴ We defer to Ref. 23 and to our paper¹⁷ for a detailed presentation of that theory. It can be applied to conformal mixing repellers and it provides the preceding estimates, namely the asymptotic scaling for the maximal eigenvalue. We would like to point

out that with our choice for the observable ψ , the perturbative approach just sketched gives the Gumbel’s law in a very direct and natural manner.

The computation of q_0 proceeds now as in Ref. 17 with a substantial difference: the nature of the conformal measure does not imply necessarily that the ratio $\frac{\nu_\beta(B(Tx,r))}{\nu_\beta(B(x,r))}$ is constant, which happened when the conformal measure was Lebesgue. This difficulty could be partially overcome by supposing that the potential is constant, otherwise we could bound q_0 from above and below with (close) approximations of the potential. By assuming that the latter is constant and equal to $\bar{\varphi}$ and also that the density h_β does not vary too much, we get that q_0 is of order $e^{\bar{\varphi}}$ and therefore

$$\theta \sim \frac{1 - \lambda_\beta^{-2} e^{\bar{\varphi}}}{\lambda_\beta^2}. \tag{2.5}$$

It is worth mentioning that whenever the conformal measure is Lebesgue ($\beta = 1$), the above computation can be made rigorous as in Proposition (5.3) in Ref. 17 and it gives

$$\theta = 1 - \frac{\int_M \frac{h^2(x)}{|T'(x)|} dx}{\int_M h^2(x) dx}, \tag{2.6}$$

where h is the density of the invariant measure: we defer to our paper¹⁷ for the assumptions on the system which permit to get such a result. In particular, those systems contain conformal repellers with finitely many branches and absolutely continuous conformal measures. Notice that by introducing the invariant measure $\mu = hdm$, we could identically write

$$\theta = 1 - \frac{\int_M h(x)e^{-\log|T'(x)|} d\mu(x)}{\int_M h(x)d\mu(x)}. \tag{2.7}$$

If the derivative does not change too much, we get $\theta \sim 1 - e^{-\Lambda_\mu}$, where Λ_μ is the positive Lyapunov exponent of the measure μ . Alternatively, if the density h could be considered constant, we can bound (2.7) by Jensen’s inequality as

$$\theta \sim 1 - \int_M \frac{1}{|T'(x)|} d\mu(x) \leq 1 - e^{-\int_M \log|T'(x)|d\mu(x)} = 1 - e^{-\Lambda_\mu}.$$

In both cases, the DEI θ is related to the positive Lyapunov exponent: this analogy will be pursued in Sec. II C.

C. Attractors and high dimensional systems

For invertible maps generating attractors endowed with the SRB measure, the computation of the dynamical extremal index is less straightforward; we should stress that a spectral theory of extreme value for (invertible) uniformly hyperbolic maps is still missing. Suppose we take an hyperbolic diffeomorphisms T preserving the ergodic SRB measure \mathcal{L} . Then, the quantity q_0 in (2.4) becomes

$$q_0 = \lim_{n \rightarrow \infty} \frac{\int d\mathcal{L}(x) \int \mathbf{1}_{S_n}(x, T^{-1}y) \mathbf{1}_{S_n}(Tx, y) d\mathcal{L}(y)}{\int d\mathcal{L}(x) \int \mathbf{1}_{S_n}(x, y) d\mathcal{L}(y)}. \quad (2.8)$$

When we iterate backward the points $y \in B(Tx, e^{-u_n})$, we should keep only those points whose preimage is at a distance at most e^{-u_n} from x . Those preimages form a set $Q(x)$ which is obtained by squeezing the ball $B(Tx, e^{-u_n})$ along the unstable manifolds. Let us suppose that the tangent expanding subspace $\Sigma_u(Tx)$ at x has dimension d . Then the measure of $Q(x)$, and therefore, by the forward invariance of the measure, of its image in $B(Tx, e^{-u_n})$ will be of order $|\det(DT(x)|_u)|^{-1} \mathcal{L}(B(Tx, e^{-u_n}))$, where $DT(x)|_u$ is the derivative of T restricted to $\Sigma_u(x)$. We remember in fact that the conditional SRB measure on the unstable manifolds is smooth. This immediately gives q_0 of order

$$q_0 \sim \frac{\int d\mathcal{L}(x) |\det(DT(x)|_u)|^{-1} \mathcal{L}(B(Tx, e^{-u_n}))}{\int d\mathcal{L}(x) \mathcal{L}(B(x, e^{-u_n}))}. \quad (2.9)$$

We see that q_0 contains information about the dimension through the scaling of the denominator; we are now interested in the contribution of the other term in the numerator. In this regard, we first remind that, for SRB measures, we can use the Pesin’s formula²⁵

$$\int d\mathcal{L}(x) |\det(DT(x)|_u)| = \sum_{j=1}^d \Lambda_j^+ = h_{\mathcal{L}},$$

where Λ_j^+ is the positive Lyapunov exponents with multiplicity one, and $h_{\mathcal{L}}$ is the metricentropy of the SRB measure. We now proceed under two assumptions as we did at the end of Sec. II B. Let us first assume that the derivative along the unstable subspaces does not vary too much. Then, we could estimate the DEI as

$$\theta \sim 1 - e^{-h_{\mathcal{L}}}. \quad (2.10)$$

For $d = 1$, we can replace the entropy with the (unique) positive Lyapunov exponent $\Lambda_{\mathcal{L}}$; in the following, we will simply write it as Λ_+ .

The other assumption exploits the fact that for these system, and for \mathcal{L} -almost all points x we have, by Young’s theorem,²⁶ that $\lim_{r \rightarrow 0} \frac{\log \mathcal{L}(B(x,r))}{\log r} = D_1$, where D_1 is the information dimension. Hence, we could guess that $\mathcal{L}(B(x, e^{-u_n})) \sim e^{-u_n D_1}$ and therefore forget about the dependence on the variable x . This is generally false since the multiplicative factor in the previous scaling could depend on x . Indeed, when we integrate $\mathcal{L}(B(x, e^{-u_n}))$, we get D_2 which could be different from D_1 . If we suppose that the dependence on x of the prefactors is negligible, which means that we are considering a homogenous fractal invariant set with $D_1 \sim D_2$, then we have for the DEI

$$\begin{aligned} \theta &\sim 1 - \int d\mathcal{L} |\det(DT(x)|_u)|^{-1} \leq 1 - e^{-\int d\mathcal{L}(x) |\det(DT(x)|_u)|} \\ &= 1 - e^{-h_{\mathcal{L}}}, \end{aligned} \quad (2.11)$$

where the derivative is *not* supposed to be constant and where we have used again the Jensen’s inequality to establish the upper bound.

Those two approximations are very crude; we are in fact either neglecting the contributions of the prefactors in the local scaling of the balls in (2.9), or not taking into account the geometric factors when the ball $B(Tx, e^{-u_n})$ is squeezed at a distance e^{-u_n} from x . Moreover, the variation of the derivative, especially sensible in the non-uniformly hyperbolic setting, could give large differences in the determination of the DEI, as we experience for instance for the Hénon map, see below. The preceding relation is pretty well satisfied for maps with one-dimensional unstable subspace and (piecewise) constant jacobian, like the Baker transformation, the Lozi map, and the solenoid. For the algebraic automorphism of the torus (cat’s map), a simple argument allows us to improve the previous rate just by taking into account the geometric factors. Surprisingly, relation (2.11) is pretty well satisfied in the example below of the generalized Hénon maps, where the unstable subspace has dimension larger than one, i.e., we have more than one positive Lyapunov exponent. In conclusion, our index θ traces in a satisfactory way the entropy. The eventual deviations are due to the variation of the derivative and the local scaling of balls in (2.9). Although these effects are difficult to compute analytically, the DEI θ is relatively easy to compute numerically and it furnishes a new indicator for the local instability in chaotic systems.

III. NUMERICAL COMPUTATIONS

The numerical computations presented in the remaining of this work are performed by using the numerical algorithms and codes detailed in the [supplementary material](#). The stability of the results is checked against different l, n, m, s . In particular, we perform two sets of simulations. The first set of accurate simulations consist of $l = 100$ trajectories, with $n = 10^6$ iterations, $m = 10^3$ blocks of $s = 10^3$ length each. The second set of $l = 100$ simulations consists of short series of $n = 10^4$ iterations, with $s = m = 10^2$. This second set is useful to check whether the technique is reliable also for short time series. Except where specified, we use $\tilde{s} = 0.99$ for the following computations. However, results are stable when considering different quantiles ranging from $0.97 < \tilde{s} < 0.999$.

A. Low dimensional maps

We begin the numerical computations with several examples on low dimensional maps. A summary of the results for all maps analysed is reported in Table I. For a few maps, we report the model equations in the [supplementary material](#) to streamline the exposition.

- Let us begin with the Bernoulli Shift map $T(x) = 3x \text{-mod } 1$. For this system, $D_2 = 1$ and $\theta = 1 - 1/3 = 2/3$. The numerical estimates (Table I) are coherent with the theoretical values for both accurate and short simulations.
- We now consider the Gauss map $T(x) = \frac{1}{x} \text{-mod } 1$ defined on the unit interval. Although, strictly speaking, this map

TABLE I. Estimates of correlation dimension D_2 and dynamical extremal index (DEI) θ obtained with $l = 100$ trajectories, consisting of $n = 10^6$ iterations or $n = 10^4$ iterations. The maxima of $\psi(x, y)$ are extracted in the block of $s = 10^3$ and $s = 10^2$ length, for a total of $m = 10^3$ or $m = 10^2$ blocks. The quantile for the estimate of the DEI is $\tilde{s} = 0.99$. For the Arnold Cat's map, the convergence to theoretical value is lower and the estimates are provided only for $\tilde{s} = 0.99999$ and $n = 10^7$.

Map	D_2 (classical)	$D_2 (n = 10^6)$	$D_2 (n = 10^4)$	θ (from Lyapunov)	$\theta (n = 10^6)$	$\theta (n = 10^4)$
Bernoulli's shifts	1	1.00 ± 0.02	1.01 ± 0.14	0.667	0.668 ± 0.004	0.69 ± 0.04
Gauss map	1	1.00 ± 0.03	0.96 ± 0.16	0.773	0.773 ± 0.005	0.78 ± 0.04
Cantor IFS	0.667	0.64 ± 0.01	0.59 ± 0.13	0.5	0.502 ± 0.005	0.50 ± 0.05
Baker map	1.41	1.46 ± 0.02	1.42 ± 0.25	0.47	0.49 ± 0.02	0.50 ± 0.04
Lozi map	1.38	1.39 ± 0.11	1.29 ± 0.25	0.37	0.37 ± 0.01	0.37 ± 0.05
Henon map	1.22	1.24 ± 0.03	1.13 ± 0.25	0.34	0.43 ± 0.01	0.43 ± 0.06
Solenoid $a = 1/3$	1.6309	1.64 ± 0.04	1.55 ± 0.17	0.5	0.51 ± 0.01	0.59 ± 0.03
Solenoid $a = 1/4$	1.5	1.52 ± 0.03	1.57 ± 0.20	0.5	0.51 ± 0.01	0.53 ± 0.03
Arnold Cat's map	1.987	2.00 ± 0.06	...	0.51	0.53 ± 0.06	...

does not fit the assumptions in Ref. 17 since in the latter paper, we consider maps with finitely many branches, we still try formula (2.6). For the Gauss map, the density is explicit and reads $h(x) = \frac{1}{\log 2} \frac{1}{1+x}$. The integral in (2.6) can be easily computed and gives $\theta = 4 \log(2) - 2 \sim 0.77$, whereas D_2 is expected to be 1. The numerical estimates are coherent with the theoretical values (Table I).

- Returning to a map with constant slope 3, we now look at the transformation generating the classical ternary Cantor set. In order to compute numerically the GEV function, one should access the invariant Cantor set, which is of zero Lebesgue measure. We need therefore to use the backward iterates of the map (otherwise almost all the forward orbits will fall into the holes), and the measures allowing us to compute the time averages are the so-called *balanced measures*, given suitable weights to the preimages of the map: see our article, Ref. 27 Sec. 3.2.2 for a description of such measures. For the ternary Cantor set and choosing equal weights $1/2$ for the two preimages, it is easy to check that such a balanced measure coincides with the Gibbs measure with $\beta = \log 2 / \log 3$ which is the Hausdorff dimension of the invariant set. The measure μ_{d_H} is called *uniform*, see Ref. 20, Sec. 3. The potential φ will be equal to $-\log 2$ and $\lambda = 1$, since by Bowen's formula $Q(d_H) = 0$. Therefore, for the ternary Cantor set, we get a DEI equal to 0.5 which is perfectly confirmed by the numerical simulations (Table I).
- For the Lozi map: $x_{n+1} = a|x_n| + y_n + 1, y_{n+1} = bx_n, a = 1.7, b = 0.5, \Lambda_+$ is of order 0, 47,²⁸ which gives, with our approximation, a DEI of order $\theta = 0.37$. Previous numerical computations for D_2 gave $D_2 \sim 1.38$.²⁹ Our computations (Table I) are coherent with the theoretical values.
- For the Hénon map $x_{n+1} = ax_n^2 + y_n + 1, y_{n+1} = bx_n, a = 1.4, b = 0.3, \Lambda_+$ is of order 0, 42,²⁸ which gives, with our approximation, a DEI of order $\theta = 0.34$. Previous numerical computations for D_2 gave $D_2 \sim 1.22$.²⁹ The GEV computations give $D_2 = 1.24 \pm 0.03$ but $\theta = 0.43 \pm 0.01$ for $n = 10^6$ (See Table I for the results with $n = 10^4$ iterations). The discrepancy of the DEI estimate does not get any better with the increase of \tilde{s} or n . As said before, we do not expect θ to coincide with the estimate 0.34 due to the variation of the derivative and the non-uniform hyperbolicity of the map.

- Let us consider the cat's map with the associated matrix $\begin{pmatrix} 1 & 1 \\ 1 & 2 \end{pmatrix}$. The stable and unstable manifolds for such a map are orthogonal, so we could suppose that the preimage of the ball $B(Tx, e^{-u_n})$ will intersect the ball $B(x, e^{-u_n})$ in a rectangle $R(x)$ centered at x and with the shortest side of length $(\lambda_+)^{-1} e^{-u_n}$, where $\lambda_+ = \frac{3+\sqrt{5}}{2}$ is the eigenvalue larger than 1 corresponding to the unstable direction. An elementary calculation shows immediately that $q_0 \sim \mathcal{L}(R(x)) / \mathcal{L}(B(x, e^{-u_n}))$ is approximately given by $\frac{4}{\pi} (\lambda_+)^{-1}$ which gives an extremal index as 0.51. Previous numerical computations for D_2 gave $D_2 \sim 1.987$.²⁹ The numerical computation with the GEV fitting gives $D_2 = 2.00 \pm 0.06$ and $\theta = 0.552 \pm 0.005$ for $n = 10^6$. In order to investigate the discrepancy with our theoretical estimate, we raised the quantile from $\tilde{s} = 0.99$ to $\tilde{s} = 0.999$, i.e., we select more extreme clusters. The estimates for this case are $\theta = 0.54 \pm 0.02$, more compatible with the theoretical one. Finally, if we consider longer trajectories ($n = 10^7$ iterates) with an even higher quantile ($\tilde{s} = 0.99999$), we get $\theta = 0.53 \pm 0.06$, which is even closer to the theoretical guess.
- We now consider the baker's map (see [supplementary material](#)); it depends on three parameters $\alpha, \gamma_a,$ and γ_b . The positive Lyapunov exponent is given by Ref. 20, Eq. (5.14)

$$\Lambda_+ = \alpha \log \frac{1}{\alpha} + (1 - \alpha) \log \frac{1}{1 - \alpha}.$$

With the value $\alpha = 1/3, \gamma_a = 1/5, \gamma_b = 1/4$, we get $\Lambda_+ \sim 0, 64$ which gives, with our approximation, an extremal index of order 0, 47. In the paper, Ref. 20 Eq. (5.18), we gave an implicit formula expressing D_2 as a function of α and with respect to the SRB measure. For $\alpha = 1/3$, this estimate reads $D_2 \simeq 1.41$. The GEV estimates are given in Table I and are consistent with the theory.

- We next consider an attractor embedded in \mathbb{R}^3 , the so-called solenoid, see [supplementary material](#); it depends upon the parameter $a \in (0, 0.5)$. The attractor is foliated by one-dimensional unstable manifolds, while each meridional disk is a two-dimensional stable manifold each of which intersecting the attractor over a Cantor set. The Lyapunov exponents are

$$\Lambda_- = \log a < 0, \quad \Lambda_+ = \log 2,$$

while the Hausdorff dimension d_H is given by the formula³⁰

$$d_H = 1 + \frac{\log 2}{-\log a}.$$

The numerical computations for the solenoid provide a further test of the validity of the numerical algorithm and are provided in Table I.

B. High dimensional generalized Hénon maps

We now analyze the generalized Hénon maps defined in Ref. 31 and further analyzed in Ref. 32. They are defined as

$$x_{n+1}(1) = ax_n(d-1)^2 - bx_n(d) \quad x_{n+1}(i) = x_n(i-1). \quad (3.1)$$

When the parameter $a=1.76$, the number of positive Lyapunov exponents is $d-1$; we could therefore test our relation (2.11) by computing the entropy $h_{\mathcal{L}}$ as the sum of positive Lyapunov exponents (see Table II in Ref. 32) for a given d . We also perform the computation of the dimension D_2 and compare it to the Kaplan-Yorke dimension D_{KY} given in Ref. 32; we used such a dimension because we did not find an explicit computation of D_2 in the literature. The good agreement between our numerical results (Fig. 1) confirm the validity of Eq. (2.10) with the caveat that an exact correspondence cannot be derived for the geometric factor that stretch balls in phase space in different dimensions: the origin of this discrepancy has been discussed in detail at the end of Sec. II C.

C. Application to atmospheric data

We now consider an application to atmospheric data. The purpose of this application is to show that the applicability of the technique on real data provides results that have a

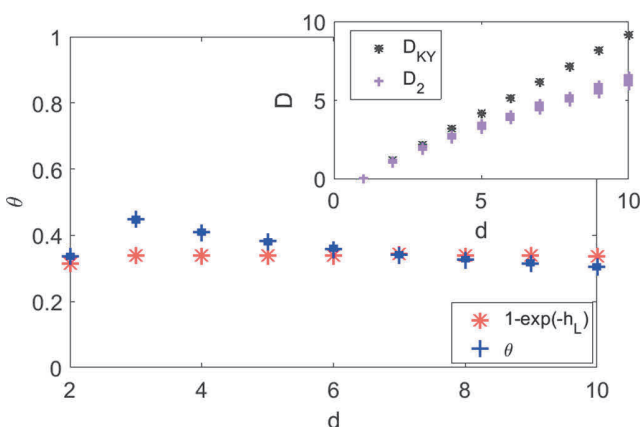


FIG. 1. Estimates of the dynamical extremal index θ and correlation dimension D_2 (inset) obtained for the Generalized Henon maps [Eq. (3.1)] in different dimensions d . The values represent the estimates obtained taking 30 couples of trajectories, iterated for $n = 10^6$ iterations. Each couple is displayed using a single marker, but the uncertainty is so small that the difference between couples is hardly recognizable. The quantile used for the estimation is $\tilde{s} = 0.98$. The results are compared to those obtained using the Kaplan-Yorke dimension D_{KY} and the entropy $h_{\mathcal{L}}$. This map has $d-1$ positive Lyapunov exponents.

coherent interpretation in terms of the underlying physics of the systems. In order to provide evidence of the robustness of our results, we will study several trajectories of a climate models which incorporate observations of the past 110 years, and compute θ and D_2 for several sub-periods showing that the results are numerically stable. We study the atmospheric circulation over the North Atlantic and focus on a single field that represents its major features: the sea-level pressure (SLP).^{33,34} Indeed, it has been shown that SLP fields can be used to study teleconnection patterns as well as storm track activity and atmospheric blocking.^{35,36} The trajectories of our dynamical systems are successions of SLP fields extracted with daily frequency from the ERA-20 CM reanalysis project over the period 1900–2010.³⁷ The ERA-20 CM consists of 10 members ensemble of a (climate) model whose task is to reconstruct at best the 1900–2010 atmospheric dynamics by constraining the model to include the information from available surface observations. Each member of the ERA 20CM is therefore a slightly perturbed reconstruction of the atmospheric dynamics in the past 110 years. The choice of the North Atlantic domain ($80^\circ \text{ W} \leq \text{Long.} \leq 50^\circ \text{ E}$, $22.5^\circ \text{ N} \leq \text{Lat.} \leq 70^\circ \text{ N}$) is motivated by the better observational coverage over the region in the first part of the analysis period compared to other regions of the globe.³⁸ Before presenting the results for D_2 and θ , we would like to stress that (i) our analysis will only be representative of the North-Atlantic domain and D_2 will be a proxy of the active degrees of freedom of the atmospheric circulation in this area. Therefore, our results cannot be used to estimate the dimension of the full atmospheric climate attractor. (ii) Previous results^{15,39,40} have shown that the estimates obtained for the daily dimensions are robust with respect to the changes in the datasets, resolution of the climate models, and are linearly insensitive to the size of the domain. This gives us confidence on the applicability of the numerical algorithm described in this paper for climate data since it is largely based on those used in Refs. 15, 39, and 40.

The results for D_2 and θ on the SLP fields of the ERA-20 CM ensemble are presented in Fig. 2. For each estimate, we fix the reference trajectory x as the first member (M1) of the ERA-20 CM ensemble because this is always considered as the reference simulation, while y is alternatively set as the M_i th member with $i = 2, 3, \dots, 10$. The dependence of the results on the reference member are tested in the [supplementary material](#) Fig. S1. To test the robustness of the results, we provide four estimates of D_2 and θ : (i) using the full data in the period 1900–2010, (ii) using 1900–1955 data, (iii) using 1900–1928 data, and (iv) considering only the first 14 years (1900–1914) of data. For each member, the results are reported in Fig. 2. The ensemble averages of D_2 and θ for the different periods are instead reported in Table II. Estimates are consistent for different periods and the value of $D_2 \simeq 9$ found on average, is slightly lower than the estimates of d_H found in Ref. 15 (we remind that $D_2 < d_H$). The value of D_2 roughly corresponds to the number of spatial degrees of freedom active in a North-Atlantic SLP field as explained in Ref. 15. Indeed, the domain used for this analysis can host about 9 large spatial structures reparted between 3 and 4 extratropical cyclones at time and the same number

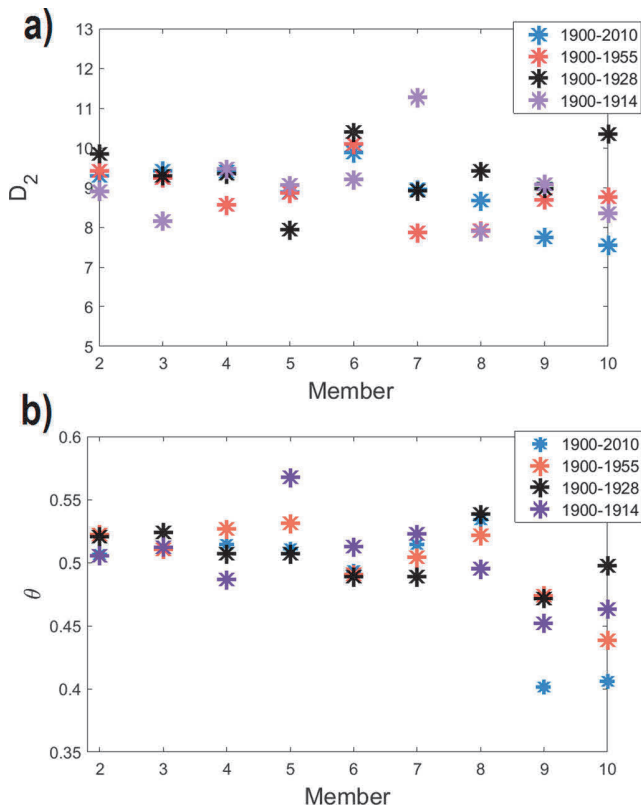


FIG. 2. Estimates of correlation dimension D_2 (a) and extremal index θ (b) obtained for daily sea-level pressure maps for four different periods in the ERA-20CM reanalysis. The values represent the estimates obtained taking as reference trajectory x the member M1 and as y , the remaining 9 ensemble members.

of anticyclones (see the textbook of Holton,⁴¹ for estimates of the typical size of these objects). θ is, in fact, the inverse of the average time the two trajectories x and y cluster together. The value of the DEI $\theta=0.5$ corresponds therefore to a contraction of the phase space associated with a time-scale between 2 and 3 days. This is the typical decay rate of baroclinic eddies associated with the low pressure systems observed in SLP fields (see again the textbook by Holton⁴¹ for the decay rates). We finally notice that our formula (2.11) gives for the entropy the value $\log 2$. In Fig. S2, we show a moving window computation of D_2 and θ . No clear trend emerges that could be attributed to anthropogenic forcing. This result is consistent with those found for d_H in Ref. 39. We remark however some differences in the variability of

TABLE II. Estimates of correlation dimension D_2 and extremal index θ obtained for daily sea-level pressure maps for four different periods of the ERA-20CM reanalysis. The values represent average over the 9 ensemble members and uncertainty is expressed as the standard deviation of the ensemble mean.

Period	D_2	θ
1900-2010	8.9 ± 0.8	0.48 ± 0.05
1900-1955	8.8 ± 0.7	0.50 ± 0.03
1900-1928	9.4 ± 0.8	0.50 ± 0.02
1900-1914	9.0 ± 1.0	0.50 ± 0.03

the indicators among the members. In particular, M9 and M10 have a minimum of θ around 1960. This could be due to the different boundary conditions applied to the members and detailed in Ref. 37.

D. Additive noise

In our previous papers,^{17,42,43} we have analyzed the effect of additive noise on the parameters of the extreme value laws. It consists in defining a family of maps $T_\xi = T + \varepsilon \zeta$ with ζ a random variable sampled from some distribution \mathbb{G} (we will take here the uniform distribution on some small ball of radius ε around 0). The iteration of the single map T will be now replaced by the concatenation $T_{\xi_n} \circ T_{\xi_{n-1}} \cdots \circ T_{\xi_1}$ and the evaluation of an observable computed along this orbit will be given by the probability measure \mathbb{P} which is the product of \mathbb{G}^N with the so-called *stationary measure* μ_s , verifying, for any real measurable bounded function f : $\int f d\mu_s = \int f \circ T_\xi d\mu_s$; see Ref. 19 Chap. 7, for a general introduction to the matter. In the aforementioned papers, Refs. 42 and 43, we have shown analytically that for dynamical systems perturbed additively, the extremal index $\theta=1$, no matter what the intensity of the noise is. The proof was supported by numerical experiments, using also different noise types. The extremal index is a parameter that quantifies the amount of clustering, the stickiness of the trajectory in phase space. In our setting, clustering happens in the presence of invariant sets, which are periodic points in Ref. 42. By looking at formula (2.4), we see that we estimate the proportion of the neighborhood of the invariant set returning to itself; as we argued above, that estimate gives information on the rate of backward volume contraction in the unstable direction. Since the noise generally destructs these invariants sets, we expect the extremal index be equal to 1 or quickly approaching 1 when the noise increases. This is confirmed by the numerical experiments reported in Fig. 3 where the value of θ is plotted against the intensity of the noise ε for three maps: $3x \bmod 1$ map, the Baker map, and the Lozi map. In all cases, indeed $\theta \rightarrow 1$ for large enough noise. However, with respect to the observables discussed in Ref. 42, we find some remarkable differences on the intensity of the noise needed to observe changes of the extremal index from the deterministic values: whereas in Ref. 42, we observed significant deviation from the deterministic behavior for very small noise intensities ($\varepsilon \geq 10^{-4}$), here we need $\varepsilon \geq 10^{-2}$, i.e., only large noise amplitudes perturb the estimates of D_2 and θ . This difference can be easily explained: in Ref. 42, the extremal index was used to explore the local stability at periodic fixed points, where the dynamics is deeply affected even by a small noise. Here, instead, the extremal index tracks a global property that it is stable with respect to small stochastic perturbations. We underline that, for the Lozi map, we cannot obtain estimates of θ for noise larger than 0.1 because the dynamics falls out the basin of attraction.

IV. DISCUSSION AND CONCLUSIONS

Using the extreme value theory, we have introduced a new and efficient way to compute the correlation dimension

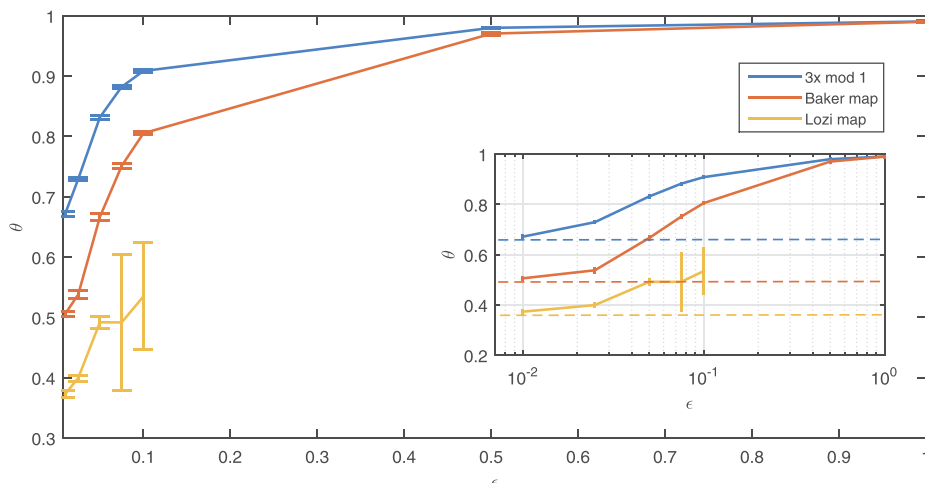


FIG. 3. Dynamical extremal index θ vs intensity of the additive noise ϵ for three different maps: $3 \times \text{mod } 1$ (blue), Baker map (red), and Lozi map (orange). The error bar indicates the standard deviation of the sample of $l = 100$ trajectories, each consisting of $n = 10^6$ iterations. The quantile for the estimate of the extremal index is $\tilde{s} = 0.99$. The inset shows the same data in the semilog scale, with the deterministic values represented by the dotted lines.

D_2 . Moreover, for higher dimensional maps, we introduced the quantity q_0 , related to the expectation of the inverse of the determinant of the derivative along the expanding subspace. Therefore, the extremal index $\theta = 1 - q_0$ is a *measure of the average rate of phase space contraction for backward iteration*. Although this quantity slightly differs from the entropy or from the positive Lyapunov exponent when the expanding subspace has dimension one, it provides an important piece of information on the dynamics of the system. In fact it can be linked to the global predictability and therefore *considered as a new indicator of the local instability in chaotic systems*. We would like also to emphasize that both θ and D_2 can be computed simultaneously just by looking at the GEV function and this makes our method quite rapid and efficient from a numerical point of view. We have shown that even for a short time series of only of 10^4 iterations, the estimates are robust and consistent with the theoretical expectations. We have also presented a first application of these indicators to climate data proving that the indicators are useful to infer the spatial number of degrees of freedom and the typical time scales of the atmospheric dynamics on the North Atlantic region. Finally, we have observed their sensitivity to the different boundary conditions imposed for the climate simulations analyzed. This implies that the indicators could be useful in characterizing and comparing also different climate datasets as those analyzed in international campaigns.

Our interpretation of θ together with that on the correlation dimension D_2 could be useful also to analyze the times series arising from the evolution of chaotic systems. Indeed, these quantities are particularly straightforward to obtain from numerical computations. Moreover, the results obtained can also be used to detect the embedding dimension, namely by replacing the sample of data with delay vectors of variable lengths; we stress that computing the GEV with those delay vectors will allow us to get exactly the embedding dimension. We mean to develop further this approach in a future paper.

Finally, the computation of the DEI could be helpful to distinguish purely stochastic sequences for which the extremal index should approach 1, see Sec. III D, from dynamical systems with an underlying chaotic behavior even

in the presence of small stochastic perturbations. Again, these further applications of our approach with EVT will be the objects of forthcoming investigations.

SUPPLEMENTARY MATERIAL

See [supplementary material](#) for: (i) the algorithm for the estimation of the correlation dimension D_2 and the Dynamical Extremal Index (DEI) θ , (ii) a commented numerical MATLAB code for such estimation, (iii) the model equations for the maps used, and (iv) the supplementary figures.

ACKNOWLEDGMENTS

S.V. was supported by the MATH AM-Sud Project Physeco, by the Leverhulme Trust through the Network Grant No. IN-2014-021, and by the project APEX Systèmes dynamiques: Probabilités et Approximation Diophantienne PAD funded by the Région PACA (France). D.F. was partially supported by the ERC Grant A2C2 (No. 338965). The authors warmly thank the referee whose comments and advices helped them to improve the paper.

¹P. Grassberger and I. Procaccia, *The Theory of Chaotic Attractors* (Springer, 2004), pp. 170–189.

²P. Grassberger and I. Procaccia, *Phys. Rev. Lett.* **50**, 346 (1983).

³A. Wolf, J. B. Swift, H. L. Swinney, and J. A. Vastano, *Physica D* **16**, 285 (1985).

⁴M. T. Rosenstein, J. J. Collins, and C. J. De Luca, *Physica D* **65**, 117 (1993).

⁵J. Theiler, S. Eubank, A. Longtin, B. Galdrikian, and J. D. Farmer, *Physica D* **58**, 77 (1992).

⁶J.-P. Eckmann and D. Ruelle, *Physica D* **56**, 185 (1992).

⁷H. Kantz and T. Schreiber, *Nonlinear Time Series Analysis* (Cambridge University Press, 2004), Vol. 7.

⁸A. Pikovsky and A. Politi, *Lyapunov Exponents: A Tool to Explore Complex Dynamics* (Cambridge University Press, 2016).

⁹H. Kantz, G. Radons, and H. Yang, *J. Phys. A: Math. Theor.* **46**, 254009 (2013).

¹⁰A. Politi, *Phys. Rev. Lett.* **118**, 144101 (2017).

¹¹A. C. M. Freitas, J. M. Freitas, and M. Todd, *Probab. Theory Relat. Fields* **147**, 675 (2010).

¹²D. Faranda, V. Lucarini, G. Turchetti, and S. Vaienti, *J. Stat. Phys.* **145**, 1156 (2011).

¹³D. Faranda and S. Vaienti, *Geophys. Res. Lett.* **40**, 5782, <https://doi.org/10.1002/2013GL057811> (2013).

- ¹⁴D. Faranda, M. C. Alvarez-Castro, and P. Yiou, *Clim. Dyn.* **47**, 3803 (2016).
- ¹⁵D. Faranda, G. Messori, and P. Yiou, *Sci. Rep.* **7**, 41278 (2017).
- ¹⁶F. M. E. Pons, G. Messori, M. C. Alvarez-Castro, and D. Faranda, preprint [arXiv:hal-01650250](https://arxiv.org/abs/hal-01650250) (2017).
- ¹⁷D. Faranda, H. Ghoudi, P. Guiraud, and S. Vaienti, "Extreme value theory for synchronization of coupled map lattices," *Nonlinearity* (to be published); preprint [arXiv:1708.00191](https://arxiv.org/abs/1708.00191).
- ¹⁸Y. B. Pesin, *Dimension Theory in Dynamical Systems: Contemporary Views and Applications* (University of Chicago Press, 2008).
- ¹⁹V. Lucarini, D. Faranda, J. M. Freitas, M. Holland, T. Kuna, M. Nicol, M. Todd, S. Vaienti *et al.*, *Extremes and Recurrence in Dynamical Systems* (John Wiley & Sons, 2016).
- ²⁰D. Bessis, G. Paladin, G. Turchetti, and S. Vaienti, *J. Stat. Phys.* **51**, 109 (1988).
- ²¹A. Ferguson and M. Pollicott, *Ergodic Theory Dyn. Syst.* **32**, 961 (2012).
- ²²G. Keller, *Equilibrium States in Ergodic Theory* (Cambridge University Press, 1998), Vol. 42.
- ²³G. Keller, *Dyn. Syst.* **27**, 11 (2012).
- ²⁴G. Keller and C. Liverani, *J. Stat. Phys.* **135**, 519 (2009).
- ²⁵M. Viana, *Lectures on Lyapunov Exponents* (Cambridge University Press, 2014), Vol. 145.
- ²⁶L.-S. Young, *Ergodic Theory Dyn. Syst.* **2**, 109 (1982).
- ²⁷V. Lucarini, D. Faranda, G. Turchetti, and S. Vaienti, *Chaos* **22**, 023135 (2012).
- ²⁸G. Paladin and S. Vaienti, *J. Stat. Phys.* **57**, 289 (1989).
- ²⁹J. C. Sprott and G. Rowlands, *Int. J. Bifurcation Chaos* **11**, 1865 (2001).
- ³⁰K. Simon, *Proc. Am. Math. Soc.* **125**, 1221 (1997).
- ³¹G. Baier and M. Klein, *Phys. Lett. A* **151**, 281 (1990).
- ³²H. Richter, *Int. J. Bifurcation Chaos* **12**, 1371 (2002).
- ³³J. W. Hurrell, *Science* **269**, 676 (1995); ISSN 0036-8075.
- ³⁴G. Moore, I. A. Renfrew, and R. S. Pickart, *J. Clim.* **26**, 2453 (2013).
- ³⁵J. C. Rogers, *J. Clim.* **10**, 1635 (1997).
- ³⁶L. Comas-Bru and F. McDermott, *Q. J. R. Meteorol. Soc.* **140**, 354 (2014).
- ³⁷H. Hersbach, C. Peubey, A. Simmons, P. Berrisford, P. Poli, and D. Dee, *Q. J. R. Meteorol. Soc.* **141**, 2350 (2015).
- ³⁸O. Krueger, F. Schenk, F. Feser, and R. Weisse, *J. Clim.* **26**, 868 (2013).
- ³⁹D. Rodrigues, M. C. Alvarez-Castro, G. Messori, P. Yiou, Y. Robin, and D. Faranda, *Journal of Climate* (2017).
- ⁴⁰D. Faranda, G. Messori, M. C. Alvarez-Castro, and P. Yiou, *Nonlinear Processes Geophys.* **24**, 713 (2017).
- ⁴¹J. R. Holton, *Am. J. Phys.* **41**, 752 (1973).
- ⁴²D. Faranda, J. M. Freitas, V. Lucarini, G. Turchetti, and S. Vaienti, *Nonlinearity* **26**, 2597 (2013).
- ⁴³H. Aytac, J. Freitas, and S. Vaienti, *Trans. Am. Math. Soc.* **367**, 8229 (2015).